Effect of Carbon Nanotubes on Dynamic Mechanical Properties, TGA, and Crystalline Structure of Polypropylene

Mohammad Razavi-Nouri

Iran Polymer and Petrochemical Institute, PO Box 14965/115, Tehran, Iran

Received 28 April 2010; accepted 26 February 2011
DOI 10.1002/app.34484
Published online 2 November 2011 in Wiley Online Library (wileyonlinelibrary.com).

ABSTRACT: This paper is devoted to the preparation of thermoplastic nanocomposites of polypropylene (PP) and different amounts of single-walled carbon nanotubes (SWNTs) in the range 0.25–2 wt %. The effect of SWNT content on the dynamic mechanical behavior, thermal degradation, crystalline structure, and the kinetic crystallizability of PP were studied. The results obtained from dynamic mechanical thermal analyzer (DMTA) showed that the maximum storage modulus was achieved when 1 wt % SWNT was added into the pristine polymer. Thermal stability of the nanocomposites was measured by thermogravimetric analyzer (TGA). From the TGA results, it was found that the weight fraction of PP which was located at the interface for the nanocomposite containing 0.5% SWNT was about 60%, and this value did not change much with the addition of higher amounts of SWNT. Moreover, the thickness of the interface between PP and SWNT was estimated to be of the order of 10^1 nm which is very close to the radii of gyration of PP molecular chains. Wide angle X-ray diffractometer (WAXD) was used to explore the crystalline structure of water and slow-cooled samples. It was found that the crystallization of PP in 040 lattice plane increased for the nanocomposites compared with PP for both cooling rates studied. It was also found that the kinetic crystallizability values were nearly the same for PP and the nanocomposites. © 2011 Wiley Periodicals, Inc. J Appl Polym Sci 124: 2541–2549, 2012

Key words: carbon nanotube; poly(propylene); thermogravimetric analysis

INTRODUCTION

Since the report of Iijima[1] on carbon nanotubes (CNT) in 1991, studies on the physical and mechanical properties of CNT/polymer nanocomposites have attracted many scientists attentions.[2–10] Single- (SWNT) and multi-walled carbon nanotubes (MWNT) have high aspect ratio, stiffness, and strength as well as high electrical and thermal conductivity. Composites which are produced with CNT in comparison with those are reinforced with traditional natural or synthetic fibers can be processed much easier, and the moldings have better surface appearance even if they are filled with high content of CNT.[11]

Polypropylene (PP) is among the most versatile polymer matrices with well-balanced physical and mechanical properties, easy processability and low cost. This material is a semicrystalline thermoplastic polymer, and the physical and mechanical properties of PP depend on its microstructure. The microstructure is surveyed by crystallization rate and the degree and quality of crystallization. The crystalline morphology of PP can also be dictated by the fibers (or fillers) that can act as nucleating agents, affecting the crystallization process.

It is well known that PP displays three main crystalline forms of monoclinic (α), hexagonal (β) and orthorhombic (γ). A quenched (smectic) and a less common δ-form have also been proposed.[12–14] The α-form is the most common crystalline structure. The β-phase is difficult to form unless specific nucleating agents, rapid quenching, or shear field are used to produce an enriched or the β-form alone.[12,15–18] The γ-phase can be reached for isotactic PP when crystallization occurs at high pressures or under stress.[19–21] However, γ-phase can readily be formed under atmospheric pressure when copolymers of propylene with low amount of ethylene or other 1-olefin counits are crystallized. In this case, chain defects which are introduced in isotactic sequences of PP are in favor of γ-phase formation.[22,23]

Wang et al. have developed a mesoscopic numerical tool for the prediction of the effective thermal conductivities of random porous media[24,25] and also random microstructures of carbon fiber composites[26] by using a high-efficiency lattice Boltzmann solver. In both cases, they have reported that the predicted

Correspondence to: M. Razavi-Nouri (m.razavi@ippi.ac.ir or razavinourim@yahoo.co.uk).

© 2011 Wiley Periodicals, Inc.

thermal conductivities using this method were consistent with the experimental values, indicating that the present method is a robust model for solving complex systems.

The main goals of this work are to explore the dynamic mechanical properties and thermal degradation behavior of PP and its nanocomposites reinforced with selected amounts of SWNT. The types of PP crystalline structure formed in the pristine polymer and also in the nanocomposites were studied after cooling the samples at two different cooling rates. The kinetic of crystallizability value was also calculated for PP and the nanocomposites.

EXPERIMENTAL

Materials

The raw materials were obtained from commercial sources. The isotactic PP homopolymer was supplied as the grade Poliran PI0800 by Bandar Imam Petrochemical co. (Iran). The number average molecular weight, M_n, weight average molecular weight, M_w, and polydispersity were 56, 257 kg/mol, and 4.6, respectively. The melt flow index and density were also 8 g/10min and 0.902 g/cm^3, respectively. The SWNT was provided by Research Institute of Petroleum Industry (Iran). The SWNT was prepared using a chemical vapor deposition (CVD) process, via methane as a carbon source, cobalt, and molybdenum catalyst system, and reaction temperature in the range 800–1000°C.

Preparation of nanocomposites

Prior to the preparation of nanocomposites, PP and SWNT were dried in a vacuum oven for 12 h at 80°C. Melt mixing of the components was performed in an internal mixer (Haake Rheomix; HBI SYS90) equipped with a pair of roller-type blades. After dry blending of PP granules with selected amount of SWNT, the mixture was introduced into the mixer. The rotor speed and temperature were set at 120 rpm and 180°C, respectively, and mixing continued for 10 min. A control sample of PP without SWNT was also processed under the same conditions for comparison. The mixtures were then compression molded in the shape of square plaques (0.5 mm thick) at 190°C and 10 MPa for 5 min by using a Toyoseiki Mini Test Hydraulic Press (Japan). These sheets were then quenched in two different ways. Slow-cooled sample was prepared by cooling the sample in the press. In this case, the hot press heaters were switched off and allowed the sample to cool to room temperature over 5 h under 10 MPa pressure exerted to the sample. However, to prepare water-cooled samples, the sheets were directly quenched in ice–water mixture. The formulations of the nanocomposites are presented in Table I.

TABLE I
The Samples of Nanocomposites Studied

Sample	*PP (wt %)*	*SWNT (wt %)*
PP	100	—
PP/SWNT (0.25%)	99.75	0.25
PP/SWNT (0.50%)	99.5	0.5
PP/SWNT (0.75%)	99.25	0.75
PP/SWNT (1%)	99	1
PP/SWNT (2%)	98	2

Differential scanning calorimetry

Crystallization studies were carried out using a Perkin–Elmer (Pyris 1, Waltham, Massachusetts) differential scanning calorimeter (DSC) under nitrogen atmosphere to avoid any oxidation. Each sample of 5 ± 0.2 mg was taken from the molded sheet and encapsulated in an alumina closed pan. The following procedure was used in nonisothermal conditions to reveal the crystallization behavior. The sample was heated from 50 to 210°C at a heating rate of 10°C/min, held at 210°C for 5 min to eliminate any previous thermal history, and then cooled to 50°C at a cooling rate of 10°C/min.

Dynamic mechanical thermal analyzer

Dynamic mechanical analysis (DMTA) was carried out using a Tritec 2000 DMA instrument (Triton Technology, UK) at temperature range of −120 to 160°C, heating rate of 3°C/min and frequency of 1 Hz. All the samples were tested in the single cantilever bending mode.

Thermogravimetric analysis

Thermogravimetric analysis (TGA) was performed on a Polymer Laboratories model STA 1640 (UK) under nitrogen atmosphere from ambient temperature up to 600°C with heating rate of 20°C/min.

X-ray diffraction

Wide angle X-ray diffraction (WAXD) experiments of the samples were carried out on a D500 diffractometer (Siemense, Germany) operated with CuKα radiation (λ = 1.54 Å) at 40 kV and 100 mA. The scans were recorded in the range of 2θ values from 10° to 30° in steps of 0.05°, and the count time was selected to be 1 s per step.

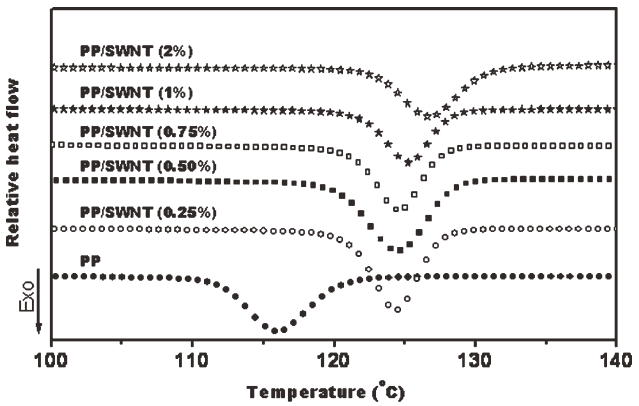

Figure 1 Schematic DSC exotherms for the determination of nonisothermal crystallization parameters.

RESULTS AND DISCUSSION

The kinetic crystallizability

The crystallization exotherms of PP and PP/SWNT nanocomposites are shown in Figure 1. The temperature of crystallization of the nanocomposites was higher than that of the pristine polymer according to heterogeneous nucleating action of SWNT in PP. This effect was more pronounced at low SWNT content, and the results published elsewhere in details.[27]

Ziabicki[28–30] suggested that the kinetics of polymer phase transportation can be represented by a first-order kinetic equation such as

$$\frac{dX}{dt} = K(T)[1 - X] \tag{1}$$

where $K(T)$ is a temperature-dependent crystallization rate function and X is the relative crystallinity calculated from DSC thermograms by the following equation:

$$X = \frac{\int_{T_0}^{T_t} \frac{dH}{dT} dT}{\int_{T_0}^{T_\infty} \frac{dH}{dT} dT} \tag{2}$$

where $\frac{dH}{dT}$ is the crystallization heat evolution rate, T_0 is the temperature at which crystallization starts, T_t is the temperature at which crystallization proceeds for time t, and T_∞ is the end temperature of crystallization.

Jeziorny[31–34] derived an equation according to Ziabicki's theory to estimate the quantity G defined as the kinetic crystallizability by means of nonisothermal crystallization:

$$G = \int_{T_g}^{T_m} K(T)dT = (\pi/\ln 2)^{0.5} K_{\max} D/2 \tag{3}$$

where $K_{\max}$ is the value of $K(T)$ at the maximum crystallization rate and D is the half-width of the crystallization peak. The parameter G characterizes the degree of transformation obtained over the entire range of crystallization from the melting point (T_m) to glass transition temperature (T_g). Considering the influence of cooling rate ($\frac{dT}{dt}$) during nonisothermal crystallization, G must be corrected as follows:

$$G_C = \frac{G}{(dT/dt)} \tag{4}$$

The parameter G_c is the kinetic crystallizability at unit cooling rate. By knowing the values of $K_{\max}$ and D appearing in eq. (3), the calculation of G_c is made possible. D can directly be estimated from the DSC crystallization peak, and $K_{\max}$ can be calculated as

$$K_{\max} = C_K / t_{\max} \tag{5}$$

where

$$C_K = \frac{\int_{t_0}^{t_{\max}} (dH/dt)dt}{\int_{t_{\max}}^{t_\infty} (dH/dt)dt} \tag{6}$$

where $t_{\max}$ is the time from the start of crystallization t_0 to the maximum rate of crystallization, and t_∞ is the time at which crystallization ends.

It should be noted that polymers with higher values of G_c crystallize more easily.[30] The parameters characterizing the nonisothermal kinetic crystallizability of PP, and the PP/SWNT nanocomposites are presented in Table II. The results show that the value of the kinetic crystallizability which is related only to the intrinsic structure of the pristine polymer[33,34] is not influenced much and remains nearly independent of the amount of SWNT used in PP.

Dynamic mechanical behavior

PP homopolymer in the range −100 to 100°C shows three relaxations, in general. The relaxation which

TABLE II
The Kinetic Crystallizability Parameters of PP and the Nanocomposites

Sample	D (K)	$K_{\max}$ (min^{-1})	G_C (± 10%)
PP	4.927	2.308	1.210
PP/SWNT (0.25%)	3.719	2.724	1.078
PP/SWNT (0.5%)	4.764	2.299	1.166
PP/SWNT (0.75%)	3.667	2.678	1.045
PP/SWNT (1%)	3.661	2.760	1.075
PP/SWNT (2%)	4.563	2.498	1.213

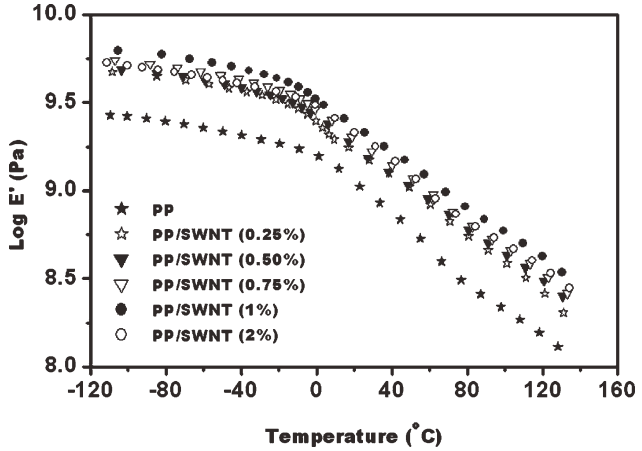

Figure 2 Variation of log E' with temperature for PP and the nanocomposites at 1 Hz.

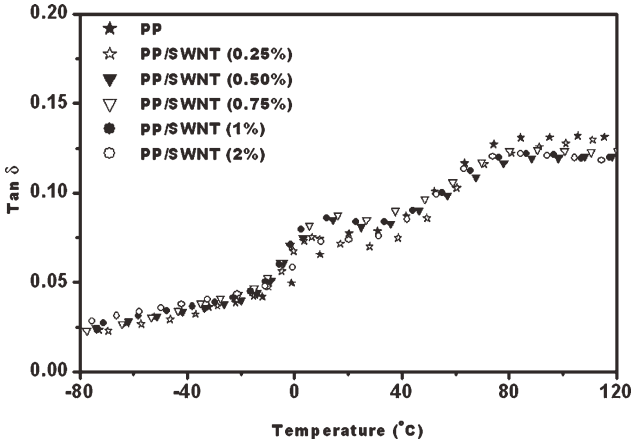

Figure 4 Variation of tan δ with temperature for PP and the nanocomposites at 1 Hz.

can be seen at the lowest temperature is related to the local mode relaxation in the amorphous phase and is known as γ-relaxation. The β-relaxation which appears at around 0°C is the dominant relaxation and corresponds to the glass-rubber transition of the amorphous phase. Another peak which usually appears as a shoulder in the range 35–90°C is attributed to the α-relaxation and can be related to the lamellar slip mechanism and also rotation within crystals.[35–37] In this work, our study was focused on the β-relaxation. The variation of storage modulus (E') against temperature for PP, and all of the nanocomposites prepared is shown in Figure 2. This figure revealed that the E' of PP increased with the addition of SWNT in the whole temperature range studied. However, the maximum storage modulus was achieved when 1% SWNT was added into PP (Fig. 3). It should also be mentioned that although the modulus has been increased significantly compared with that of PP when SWNT is added to the matrix, the reinforcement of SWNT is lower than the amount it is expected. This is because the SWNTs are not mainly distributed as single fibers into the matrix, but they are mainly dispersed in the form of bundle of fibers.[38] The reduction of the modulus at higher amount of SWNT (more than 1 wt %) into the matrix could also be attributed to the existence of SWNT aggregates which decrease the effective aspect ratio of SWNTs as well as the lower interface between PP and the nanotubes. It seems that the dispersion of the filler becomes impossible for the nanocomposites containing higher amount of nanotubes, especially by the melt mixing method. The trend of variation of E' with SWNT content at room temperature was exactly the same as we found for elastic modulus and published elsewhere.[27] Figure 4 shows the variation of mechanical loss factor (tan δ) of PP and the nanocomposites as a function of temperature. The temperature of the peak maximum which is observed at about 10°C has generally been assigned to the T_g of PP and is slightly affected by the inclusion of SWNT. It means that the β-relaxation of PP and the nanocomposites were observed at nearly the same temperatures.

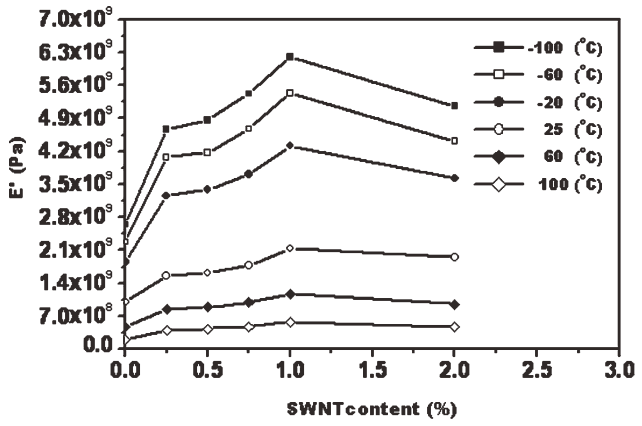

Figure 3 Variation of E' with SWNT content at selected temperatures.

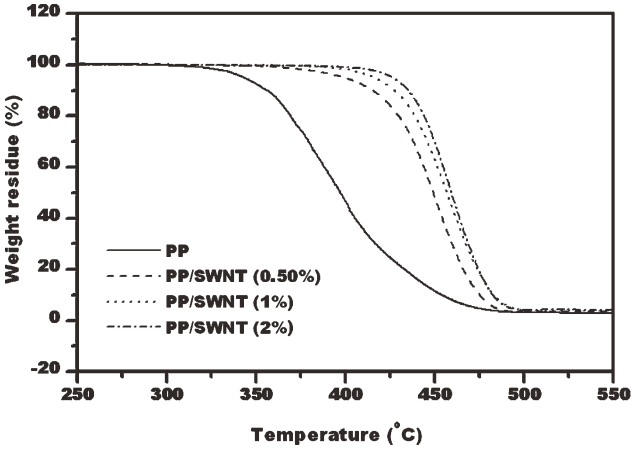

Figure 5 TGA curves for PP and the nanocomposites.

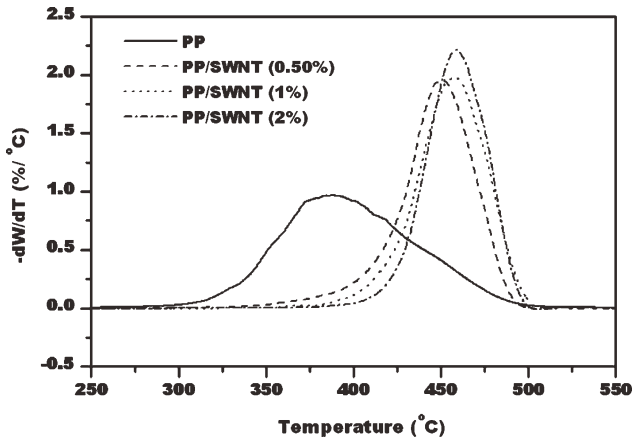

Figure 6 Variation of weight loss rate with temperature for PP and the nanocomposites.

Thermal degradation

The TGA profiles of PP and PP/SWNT nanocomposites are shown in Figure 5. As it can be seen the variation of weight with temperature follows a sigmoid-like shape for all the samples studied. In addition, all the nanocomposites prepared show higher thermal stability than that of the pristine polymer, and also thermal degradation shifts to higher temperature with the increase of SWNT. The variation of the first derivative of residual weight relative to temperature as a function of temperature is a bell-shaped curve (see Fig. 6), which has a single maximum for PP and also the nanocomposites. It was found that the onset temperature for degradation (T_{onset}) which was taken as the temperature at which the weight loss is 5% of the sample weight increased by 56, 73, and 84°C, and the temperature of the maximum weight loss rate (T_p) enhanced by 62, 69, and 71°C for the nanocomposites containing 0.5%, 1%, and 2% SWNT, respectively, compared with PP in the experimental conditions employed for this work. Therefore, it was observed that at low SWNT loading (0.5%), T_{onset} and T_p increased abruptly, and there was little increase in both temperatures when the amount of SWNT was beyond 0.5%, especially for T_p.

TABLE III
The Calculated Parameters of Gauss Distribution Function

Material	A	X_c	W
PP	93.49	395.38	77.57
PP/SWNT (0.5%)	91.47	450.23	37.98
PP/SWNT (1%)	95.80	457.07	38.75
PP/SWNT (2%)	95.33	459.26	34.21

The increase in T_{onset} and T_p has been attributed to the combination of two mechanisms. First, the barrier or labyrinth effect of the well-dispersed SWNT could prevent the transportation of the products produced from thermal degradation and thus increases the temperature at which degradation occurs. Second, this significant improvement in thermal stability of PP in the nanocomposites could also be related to the strong physical adsorption of PP molecules on the SWNT surfaces, therefore, degradation phenomena is shifted to higher temperatures.[39,40]

The bell-shaped curves of the first derivative of weight relative to temperature against temperature have been fitted by the use of a Gaussian distribution function such as

$$Y = \frac{A}{W\sqrt{\frac{\pi}{2}}}\exp\left[\frac{-2(X - X_c)^2}{W^2}\right] \quad (7)$$

where Y is the derivative of weight respect to temperature, A is the area, W is the width at half-height divided by 1.1774, X_c is the temperature at the center, and X is the temperature. All the curve fitting process reported in this work was performed using the ORIGIN 6.0 software. The experimental data and

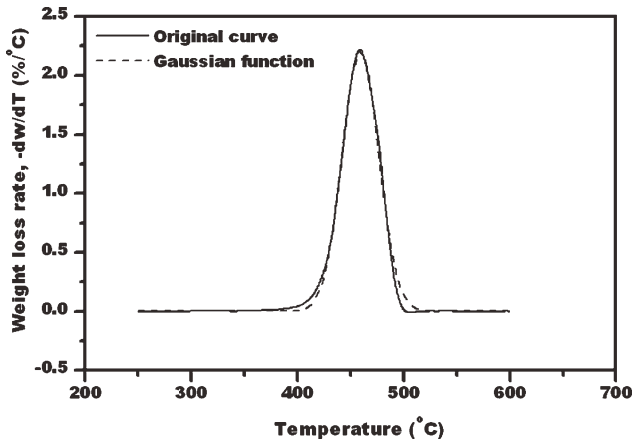

Figure 7 Experimental and the fitted curve of weight loss rate as a function of temperature for PP/SWNT (2%).

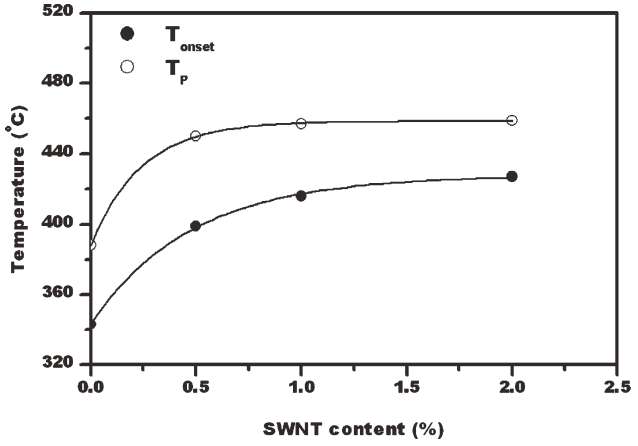

Figure 8 Experimental data (symbol) and the fitted curve (solid line) of T_{onset} and T_p against SWNT content.

TABLE IV
The Experimental and Calculated Values of T_{onset} and T_p

Sample	T_{onset} experimental (°C)	T_{onset} calculated (°C)	T_p experimental (°C)	T_p calculated (°C)
PP	343	343	388	388
PP/SWNT (0.5%)	399	398	450	450
PP/SWNT (1%)	416	417	457	457
PP/SWNT (2%)	427	426	459	459

the fitted curve obtained from the Gaussian distribution function for PP/SWNT (2%) are shown in Figure 7. It is observed that the experimental data has fairly well been fitted with the proposed equation. The calculated parameters of eq. (7) for all the materials studied are also tabulated in Table III. It is worth to mention that we have not found any physical meaning for these parameters yet.

The variation of T_{onset} and T_p with SWNT content is depicted in Figure 8. The dependence of these values on SWNT content can well be fitted by using an exponential decay function such as[41]

$$T_0 = T_1 + T_2 \exp\left(\frac{-X}{B}\right) \quad (8)$$

where $T_0 = T_1 + T_2$ is T_{onset} (or T_p) for the pristine polymer, X is the weight fraction of SWNT in the nanocomposite, and T_1, T_2, and B are constants. Fitting of the above equation to the experimental data revealed that the parameters of eq. (8) were equal to $T_1 = 427.59 \pm 1.90$, $T_2 = -84.46 \pm 2.46$, and $B = 0.47 \pm 0.04$ and also $T_1 = 458.61 \pm 0.55$, $T_2 = -70.60 \pm 0.87$, and $B = 0.24 \pm 0.01$ for T_{onset} and T_p, respectively. The T_{onset} and T_p values obtained from these fitting parameters were very close to the experimentally measured quantities for the pristine polymer and the nanocomposites (see Table IV).

The width at half-height (W_{whh}) and also the width at the baseline (W_{wbl}) of the bell-shaped curve which the latter was taken as the width between the intercept of the tangents at the baseline and the high- and low-temperature side of the curve (see insert of Fig. 9) are plotted as a function of SWNT content in Figure 9. As it can be seen, both of the quantities decreased with the increase of SWNT content. The reduction is more pronounced when 0.5% SWNT is added into PP but levels off for higher SWNT content. Decrease of the width is consistent with the fact that SWNT increase thermal conductivity of the polymer and thus make the thermal degradation process more uniform.

An equation similar to eq. (8) was employed to describe the dependence of width at half-height and width at baseline on SWNT content as

$$W_0 = W_1 + W_2 \exp\left(\frac{-X}{D}\right) \quad (9)$$

where $W_0 = W_1 + W_2$ is W_{whh} or W_{wbl} for the pristine polymer, X is the weight fraction of SWNT in the nanocomposite, and W_1, W_2, and D are constants. Figure 9 shows that eq. (9) is also capable of fitting the experimental data well. It was obtained from fitting process that $W_1 = 43.12 \pm 2.31$, $W_2 = 47.95 \pm 4.00$, and $D = 0.01 \pm 0.00$ and also $W_1 = 77.09 \pm 4.33$, $W_2 = 93.08 \pm 7.07$ and $D = 0.20 \pm 0.08$ for W_{whh} and W_{wbl}, respectively. These set of parameters are also in good agreement with the experimentally obtained values of the materials studied (see Table V). Since D is small, eq. (9) shows little sensitivity to the value of X and, thus, the same values have been obtained for W_{whh} of all the nanocomposites prepared.

Weight fraction of the polymer which is located at the interface (M_{IX}) can be estimated using the TGA data and the following equation[41]:

$$M_{IX} = \frac{M_{X0} - M_0}{M_0} \quad (10)$$

where M_{X0} is the residual weight of polymer composite containing X weight percent of SWNT at T_p of PP, and M_0 is the residual weight of PP at its T_p. Figure 10 shows the variation of weight fraction of polymer at the interface against SWNT content. The weight fraction increased abruptly at 0.5% of SWNT and remained nearly constant at higher SWNT

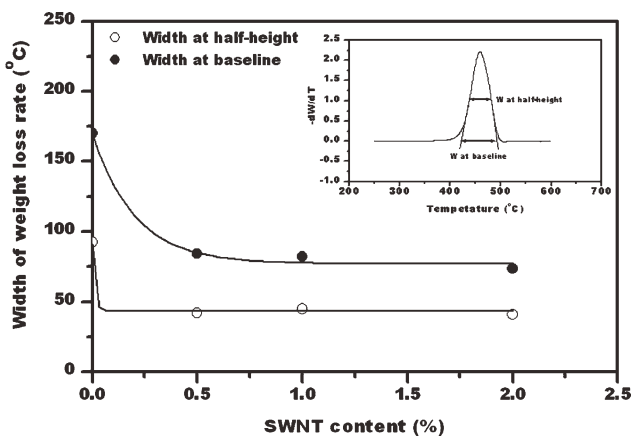

Figure 9 Experimental data (symbol) and the fitted curve (solid line) of width at half-height and width at baseline against SWNT content.

TABLE V
The Experimental and Calculated Values of W_{whh} and W_{wbl}

Sample	W_{whh} experimental (°C)	W_{whh} calculated (°C)	W_{wbl} experimental (°C)	W_{wbl} calculated (°C)
PP	92	91	170	170
PP/SWNT (0.5%)	42	43	84	85
PP/SWNT (1%)	45	43	82	78
PP/SWNT (2%)	41	43	73	77

content. Since M_{IX} is related to the thermal stability of the nanocomposites, it is now understood that why the thermal stability of the nanocomposites has not been improved as much as expected at higher loadings of SWNT. Assuming that the average length and diameter of the SWNTs used are about 2 μm and 2 nm, respectively, and also the density of PP is 0.9 g/cm^3, and that of SWNT is about 1.9 g/cm^3, the thickness of the interface between the two materials has been estimated to be of the order of 10^1 nm. This value is very close to the quantity of radii of gyration of about 30 nm which has been reported by Krause et al.[42] for PP having the molecular weight of 300 kg/mol. This is reasonably close to the molecular weight of the PP used in this study and in agreement with the fact that the thickness of the interface calculated is about the average size of the radii of gyration of PP molecular chains.

Crystalline structure

WAXD patterns of PP and PP/SWNT nanocomposites for water and slow-cooled samples are shown in Figures 11 and 12, respectively. It can be seen that the α-form is present with diffraction lines at 2θ values equal to 14.02°, 16.78°, 18.4°, 21.2°, and 21.52°. These lines represent diffraction from 110, 040, 130, 111, 131, and 041 lattice planes. The diffraction line at 21.52° is appeared because of both the 131 and 041 planes.[20,43,44] The characteristic peaks for the β- and γ-form are appeared at 2θ = 15–16° and about 19–20°, respectively. It was found that the β-crystalline structure was formed neither in the slow- nor water-cooled samples. However, while all water-cooled samples and slow-cooled PP were only crystallized in the α-form structure, a mixture of the α- and γ-form was present for the slow-cooled samples containing different amounts of SWNTs. The relative amounts of the α- and γ-crystalline form were calculated using the ratio of the intensities at 2θ value of 18.4° and 19.6°, i.e., I_α and I_γ, respectively. The fractional amount of the γ-phase in each sample was estimated from $I_\gamma/(I_\alpha + I_\gamma)$.[20,45,46] It was found that about 10% of the crystalline structure formed in all slow-cooled nanocomposites studied was in γ-crystalline form, and this value was independent of the amount of SWNT incorporated into PP. In addition, the two figures showed that the diffraction lines at 2θ = 16.78° increased in height for all nanocomposites prepared by both cooling methods, implying that introducing of SWNT increased crystallization of PP in 040 lattice plane compared with the pristine polymer. However, it was found that this effect was more pronounced for the samples prepared under slow cooling method. Therefore, the SWNT induces the crystallization of γ-form of PP, which is less stable than the α-form, and at the same time causes PP to crystallize along *b*-axis which is the normal line direction for 040 lattice plane for PP crystallized in

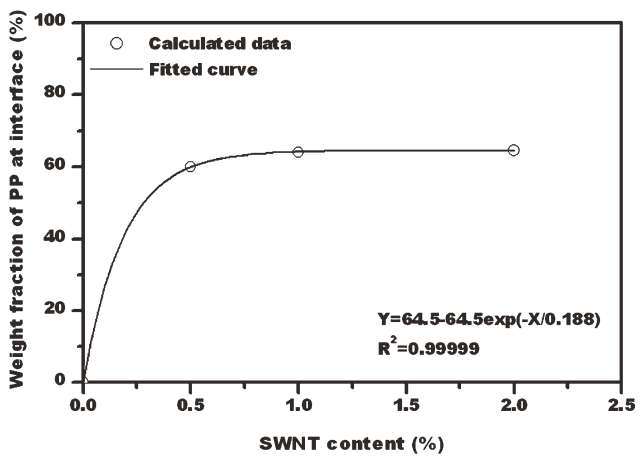

Figure 10 Calculated weight fraction of PP at interface and the fitted curve as a function of SWNT content.

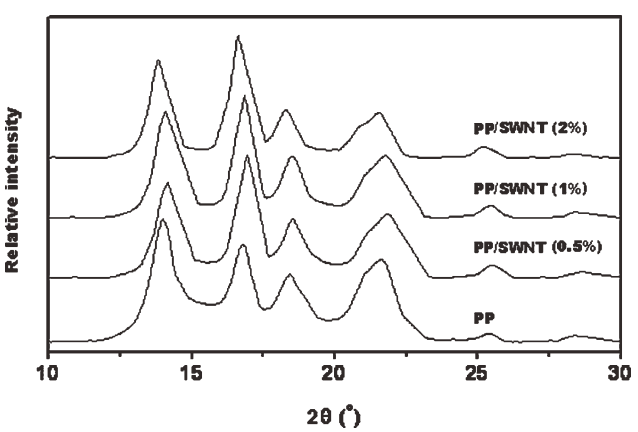

Figure 11 WAXD spectra of water-cooled PP and the nanocomposites.

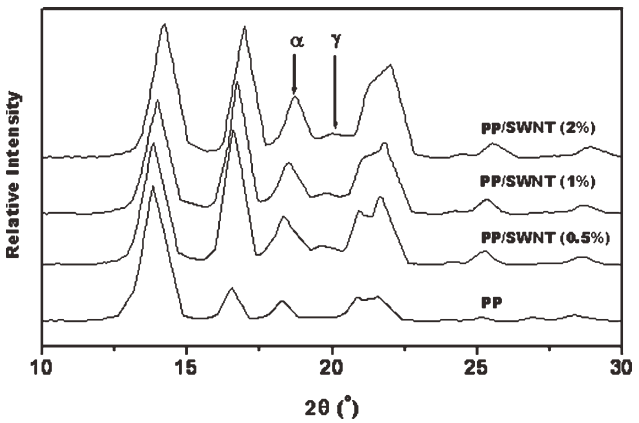

Figure 12 WAXD spectra of slow-cooled PP and the nanocomposites.

α-form.[13,44] The later means that the most preferential direction for crystal growth of PP in the nanocomposites is the 040 lattice plane. However, it seems that the growth along 110 lattice plane direction is also prevented in some extent.

CONCLUSIONS

The dynamic mechanical behavior and thermal degradation as well as crystalline structure and the kinetic crystallizability of PP were compared with that of reinforced with different amounts of SWNT. The results from nonisothermal crystallization studies showed that the kinetic crystallizability values were nearly independent of the amount of SWNT used, and they were very close to the value found for the pristine polymer. The dynamic mechanical studies revealed that the maximum storage modulus was obtained at 1% SWNT. However, the β-transition temperature did not shift much for the nanocomposites compared with that of PP. It was found from the analysis of TGA data that the Gaussian distribution function could be a suitable model to fit the experimental data of this work. In addition, the weight fraction of PP located at the interface was calculated to be in the range 60–65%, and the value was relatively independent of the amounts of SWNT incorporated into PP in the range studied. The thickness of the interface between PP and SWNT was also estimated to be in the order of 10^1 nm. This value was very close to the radii of gyration of PP chains. Studies of the crystalline structure revealed that while all water-cooled samples and slow-cooled PP showed only α-crystalline structure, some γ-crystalline structure was formed in slow-cooled PP/SWNT nanocomposites. In addition, the crystallization of PP in 040 lattice plane enhanced for all nanocomposites compared with that of the pristine polymer. Study of the degradation and response of the nanocomposites prepared open a new way to better use of the materials for more advanced technologies like aerospace and high thermal applications.

References

1. Iijima, S. Nature 1991, 354, 56.
2. Chang, T. E.; Jensen, L. R.; Kisliuk, A.; Pipes, R. B.; Pyrz, R.; Sokolov, A. P. Polymer 2005, 46, 439.
3. Abraham, T. N.; Ratna, D.; Siengchin, S.; Karger-Kocsis, J. J Appl Polymer Sci 2008, 110, 2094.
4. McNally, T.; Pötschke, P.; Halley, P.; Murphy, M.; Martin, D.; Bell, S. E. J.; Brennan, G. P.; Bein, D.; Lemoine, P.; Quinn, J. P. Polymer 2005, 46, 8222.
5. Gao, Y.; Wang, Y.; Shi, J.; Bai, H.; Song, B. Polymer Test 2008, 27, 179.
6. Dondero, W. E.; Gorga, R. E. J Polymer Sci B: Polymer Phys 2006, 44, 864.
7. Eitan, A.; Fisher, F. T.; Andrews, R.; Brinson, L. C.; Schadler, L. S. Compos Sci Technol 2006, 66, 1159.
8. Zhao, W.; Liu, Y. -T.; Feng, Q. -P.; Xie, X. -M.; Wang, X. -H.; Ye, X. –Y. J Appl Polymer Sci 2008, 109, 3525.
9. Phang, I. Y.; Ma, J.; Shen, L.; Liu, T.; Zhang, W.–D. Polymer Int 2006, 55, 71.
10. Valentini, L.; Biagiotti, J.; Kenny, J. M.; Santucci, S. J Appl Polymer Sci 2003, 87, 708.
11. Xia, H.; Wang, Q.; Li, K.; Hu, G.-H. J Appl Polymer Sci 2004, 93, 378.
12. Cheng, S. Z. K.; Janimak, J. J.; Rodriguez, J. In Polypropylene: Structure, Blends and Composites; Karger-Kocsis, J., Ed.; Chapman and Hall: London 1995; Vol.1, p 32.
13. Chen, M.; Tian, G.; Zhang, Y.; Wan, C.; Zhang, Y. J Appl Polymer Sci 2006, 100, 1889.
14. Addink, E. J.; Beintema, J. Polymer 1961, 2, 185.
15. Turner-Jones, A.; Aizlewood, J. M.; Beckett, D. R. Makromol Chem 1964, 75, 134.
16. Shi, G. -Y.; Huang, B.; Zhang, J. -Y. Makromol Chem Rapid Commun 1984, 5, 573.
17. Jacoby, P.; Bersted, B. H.; Kissel, W. J.; Smith, C. E. J Polymer Sci B: Polymer Phys 1986, 24, 461.
18. Somani, R. H.; Hsiao, B. S.; Nogales, A.; Fruitwala, H.; Srinivas, S.; Tsou, A. H. Macromolecules 2001, 34, 5902.
19. Kalay, G.; Zhong, Z.; Allan, P.; Bavis, M. J Polymer 1996, 2077, 37.
20. Feng, Y.; Jin, X.; Hay, J. N. J Appl Polymer Sci 1998, 68, 381.
21. Mezghani, K.; Philips, P. J Polymer 1997, 38, 5725.
22. Gedde, U. W. Polymer Physics; Chapman and Hall: London, England, 1995.
23. Na, B.; Lv, R.; Xu, W.; Chen, R.; Zhao, Z.; Yi, Y. Polymer Int 2008, 57, 1128.
24. Wang, M.; Wang, J. K.; Pan, N.; Chen, S. Y. Phys Rev E 2007, 75, 036702.
25. Wang, M.; Wang, J. K.; Pan, N.; Chen, S. Y.; He, J. H. J Phys D: Appl Phys 2007, 40, 260.
26. Wang, M.; Kang, Q.; Pan, N. Appl Therm Eng 2009, 29, 418.
27. Razavi-Nouri, M.; Ghorbanzadeh-Ahangari, M.; Fereidoon, A.; Jahanshahi, M. Polymer Test 2009, 28, 46.
28. Ziabicki, A. Colloid Polymer Sci 1974, 252, 433.
29. Zhao, Y. H.; Sheng, J.; Wang, Y. Q. J Appl Polymer Sci 2003, 87, 1232.
30. Supaphol, P.; Dangseeyun, N.; Srimoaon, P.; Nithitanakul, M. Thermochim Acta 2003, 406, 207.
31. Jeziorny, A. Polymer 1978, 19, 1142.
32. Wang, Y.; Liu, M.; Wang, Z.; Li, X.; Zhao, Q.; Fu, P.–F. J Appl Polymer Sci 2007, 104, 1415.
33. Bertini, F.; Canetti, M.; Ricci, G. J Appl Polymer Sci 2004, 92, 1680.
34. Canetti, M.; De Chirico, A.; Audisio, G. J Appl Polymer Sci 2004, 91, 1435.

35. Jourdan, C.; Cavaille, J. Y.; Perez, J. J Polymer Sci B: Polymer Phys 1989, 27, 2361.
36. López Manchado, M. A.; Valentini, L.; Biagiotti, J.; Kenny, J. M. Carbon 2005, 43, 1499.
37. Bikiaris, D.; Matzinos, P.; Larena, A.; Flaris, V.; Panayiotou, C. J Appl Polymer Sci 2001, 81, 701.
38. Leelapornpisit, W.; Ton-That, M. -T.; Perrin-Sarazin, F.; Cole, K. C.; Denault, J.; Simard, B. J Polymer Sci B: Polymer Phys 2005, 43, 2445.
39. Yang, J.; Lin, Y.; Wang, J.; Lai, M.; Li, J.; Liu, J.; Tong, X.; Cheng, H. J Appl Polymer Sci 2005, 98, 1087.
40. Zanetti, M.; Camino, G.; Reichert, P.; Mülhaupt, R. Macromol Rapid Commun 2001, 22, 176.
41. Chipara, M.; Lozano, K.; Hernandez, A.; Chipara, M. Polymer Degrad Stabil 2008, 93, 871.
42. Krause, B.; Stephan, M.; Volkland, S.; Voigt, D.; Häußler, L.; Dorschner, H. J Appl Polymer Sci 2006, 99, 260.
43. Zhou, Z.; Wang, S.; Lu, L.; Zhang, Y.; Zhang, Y. J Polymer Sci B: Polymer Phys 2007, 45, 1616.
44. Shangguan, Y.; Song, Y.; Zheng, Q. Polymer 2007, 48, 4567.
45. Pae, K. D. J Polymer Sci 1968 A-2, 6, 657.
46. Turner-Jones, A. Polymer 1971, 12, 487.